CHAPTER EIGHT

System Performance Characterization

MARCOS A. VAN DAM
Lawrence Livermore National Laboratory, LIVERMORE, California

8.1 INTRODUCTION

Characterizing an adaptive optics (AO) system refers to understanding its performance and limitations. The goal of an AO system is to correct wave aberrations. The uncorrected aberrations, called the residual errors and referred to in what follows simply as the errors, degrade the image quality in the science camera. Understanding the source of these errors is a great aid in designing an AO system and optimizing its performance. This chapter explains how to estimate the wavefront error terms and the relationship between the wavefront error and the degradation of the image. The analysis deals with the particular case of a Shack–Hartmann wavefront sensor (WS) and a continuous deformable mirror (DM), although the principles involved can be applied to any AO system.

8.2 STREHL RATIO

A figure of merit often used to characterize the error of an AO system is the ***Strehl ratio***, *S*. It is defined as the ratio of the maximum value of the measured point spread function (PSF) over the maximum value of the diffraction-

Adaptive Optics for Vision Science, Edited by Porter, Queener, Lin, Thorn, and Awwal

limited PSF. Consequently, the Strehl ratio lies between 0 and 1, with values greater than 0.8 corresponding to essentially diffraction-limited images. The Strehl ratio is related to the wavefront errors via the Maréchal approximation [1]:

$$S = e^{-\sigma_\phi^2} e^{-\sigma_\chi^2} \tag{8.1}$$

where σ_ϕ^2 is the wavefront phase variance and σ_χ^2 is the variance of the log-normal amplitude at the pupil plane. The amplitude varies if the pupil is not uniformly illuminated or, in the case of astronomical or horizontal path adaptive optics, if the wave propagates large distances after being aberrated, a phenomenon referred to as scintillation. The human eye is more simplistic in this regard owing to the close proximity of the optics of the eye to its pupil, which prevents the occurrence of significant scintillation effects. Equation (8.1) is accurate for root-mean-square (RMS) phase errors less than 1 radian; even when the approximation does not hold, it is still true that the larger the phase aberration, the lower the Strehl ratio. For this reason, the Strehl ratio has found widespread use in adaptive optics. Since the Strehl ratio is a function of the phase, ϕ, which is related to the wave aberration, W, via $\phi = W2\pi/\lambda$, it increases with increasing wavelength, λ. One should include the wavelength when quoting the Strehl ratio.

An AO system with a single wavefront corrector conjugate to the pupil plane, which occurs in all existing vision science systems, can only correct the wave aberrations and not the scintillation. In addition, since there is only one WS, the wave aberration is only measured at one angle, the optical axis of the WS. Hence the goal of any vision science AO system is to minimize the on-axis wavefront error.

The Strehl ratio can be used during the calibration process to gauge the image quality on a pointlike light source (hereafter called a *point source*) located where the retina of the eye would be. Measuring the Strehl ratio is more complicated than it appears [2]. Five steps are required to calculate the Strehl from well-sampled images (i.e., the core of the image is at least four pixels wide):

1. Determine the diffraction-limited PSF using Fourier optics [3]. This is relatively easy if the PSF is monochromatic but requires a weighted average over the passband if the source has a large spectral width. Normalize the PSF such that the total intensity is unity.
2. Find the maximum of the diffraction-limited PSF using some subpixel interpolation method. Fast Fourier transform (FFT) interpolation works well if the data is well sampled.
3. Find the total flux of the image. This is especially difficult when the pixel size is small and there are a lot of pixels over which to sum the intensity. Each pixel measurement has an associated error, and these errors can dominate when the number of pixels is large. Similarly, accu-

rate background subtraction is imperative: Small errors in the value of the background can result in large errors in the Strehl estimate. To reduce the error in the flux estimate, the area over which the total flux is estimated must be windowed, at the expense of overestimating the Strehl. Windows with large radii result in estimates that are noisier but less biased. Normalize the image intensity.

4. Find the maximum of the normalized image using the same interpolation method.
5. Divide the maximum value of the normalized image by the maximum value of the diffraction-limited PSF to obtain the Strehl ratio.

Another image quality metric that is commonly used is the full width half maximum (FWHM) of the image. As the name suggests, this quantity describes the angular distance between opposite points where the intensity is equal to half the peak intensity. The resulting FWHM is often called the resolution of the optical system.

The FWHM has an obvious meaning when the data is continuous and one dimensional but is more difficult to define from images, which are inherently pixelated and two dimensional. In practice, the FWHM is computed by assuming that the core of the image is approximately Gaussian. The standard deviation of the intensity distribution is calculated over a window with a length of about six standard deviations centered around the peak. The FWHM of a Gaussian is equal to 2.355 times its standard deviation.

The FWHM is hence very easy to calculate for spots with a Gaussian profile and is relatively insensitive to noise and background subtraction, since few pixels are used. The disadvantage of this metric is that it is not directly related to the wavefront error: It is much more sensitive to low-order aberrations, such as tip, tilt, and defocus than to high-order aberrations.

In the sections that follow, the wavefront error terms are presented along with a description of how to calculate them. The effect of all these wavefront errors is to reduce the Strehl ratio and to increase the FWHM of the images.

8.3 CALIBRATION ERROR

The term ***calibration error*** refers to the residual wavefront error in the absence of any external aberrations. In the absence of calibration error or aberrations external to the AO system, a point source at the location of the retina should result in a perfect diffraction-limited image in the science camera. This does not occur because there are optical aberrations in the common path and in the imaging path. A deformation can be placed on the DM during the calibration process to compensate for these aberrations: The process of estimating and applying the desired deformation is known as image sharpening (see also Chapter 7). Because some errors in the camera

can be eliminated through the image sharpening process, camera and calibration errors are bundled together.

The deformation introduced on the DM and imperfections in the lenslet array lead to the decentering of the WS spots from their nominal positions. The resulting centroids are defined to be the reference centroids (also known as centroid offsets) and are subtracted from the measured centroids when the AO loop is closed. If the reference centroids are inaccurate, for example, if the optics in the AO system are misaligned or if the measurement of the reference centroids is noisy, then there will be additional calibration errors.

The calibration error can be measured by closing the loop and simultaneously imaging a point source with no external aberrations. Then one can measure the Strehl ratio, S_{CALIB}, as described in Section 8.2 and use the Maréchal approximation to calculate the wavefront error, σ_{CALIB}.

However, images of a point source contain much more information that just the wavefront error: It is also possible to derive the wavefront itself. Phase retrieval algorithms estimate the amplitude and phase at the pupil plane from intensity measurements at the image plane and knowledge of the size of the pupil [4, 5]. Additional constraints, such as prior information about the wavefront or amplitude of the pupil or noise in the image can be incorporated in the algorithm. The disadvantage of this class of algorithms is that if the pupil is symmetric, there is an ambiguity about the sign and the orientation of the phase so this information cannot be easily used for image sharpening [6]. For example, images acquired through a circular pupil that have a positive or a negative defocus aberration look identical. In addition, these algorithms work best if a point source is being imaged. Both these issues can be resolved by implementing phase diversity [7, 8]. Here, two images are captured: one at the focal plane and one slightly out of focus. The extra information obtained allows one to resolve the ambiguity problem and also to estimate the object if it is not a point source [9]. The resulting phase estimate can be fed back to improve the calibration of the system. For example, a phase diversity algorithm by Loefdahl and Scharmer is employed at Keck Observatory to remove low-order aberrations [10].

8.4 FITTING ERROR

The ***fitting error*** is defined to be the component of the wave aberration that the DM cannot fit. This error depends on the spatial characteristics of the aberrations to be corrected and on the spatial characteristics of the DM, such as the spacing, influence function, and stroke of the actuators.

To a good approximation, a continuous DM such as those produced by Xinetics can be thought of as a high-pass spatial filter with a cutoff spatial frequency given by the Nyquist criterion of the actuator positions (the inverse of twice the spacing between adjacent actuators). Then any power in the power spectral density at spatial frequencies lower than the Nyquist criterion

will be corrected while any spatial frequencies higher will contribute directly to the fitting error [11]. This implicitly assumes that the actuator influence is a sinc (the Fourier transform of a rectangle function) interpolator, which is only approximately true. Hence the fitting error will be larger in practice.

If the actuator influence function and the wave aberration are known, the fitting error can be found by doing a least-squares fit of the actuator influence functions to the wavefront. The residual is the fitting error.

If the AO system has a WS with a finer spatial resolution than the DM (e.g., a Shack–Hartmann WS with the length of the lenslets smaller than the interactuator spacing), then the residual centroid data can be used to estimate the fitting error up to the Nyquist sampling rate of the WS. A set of many residual centroid measurements, $\mathbf{s}[n]$, is taken when the loop is closed on the eye, and these measurements averaged across the frames, giving $\bar{s}$. The component that can be corrected by the AO system is removed to give the uncorrectable residual,

$$\tilde{s} = \bar{s} - \mathbf{M}\mathbf{R}\bar{s} \tag{8.2}$$

where $\mathbf{M}$ is the influence matrix formed by pushing the actuators one by one and measuring the centroids and $\mathbf{R}$ is the reconstruction matrix. The final step is to convert $\tilde{s}$ into a wavefront by using a geometric zonal reconstructor [12, 13]. Figure 8.1 shows the fitting error observed on one subject's eye using

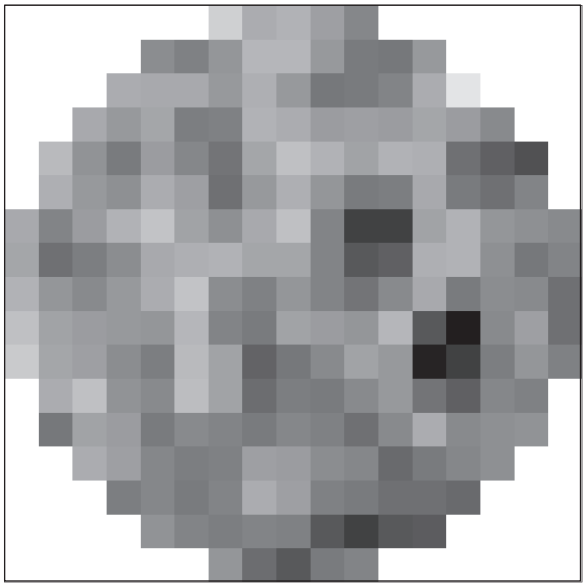

FIGURE 8.1 The fitting error over the 6.5-mm pupil of an eye using the Indiana University AO system. The RMS fitting error is 41 nm.

the AO system at Indiana University, which has 37 actuators and 221 subapertures. The RMS value of this wavefront was found to be 41 nm and this is the fitting error, σ_{FITTING}.

8.5 MEASUREMENT AND BANDWIDTH ERROR

The two remaining sources of error to be described in this chapter are ***measurement error*** and ***bandwidth error***. The measurement error term is due to noise in the wavefront slope measurement propagating through the control loop to the mirror. The bandwidth error is due to the component of the turbulence that is not compensated by the AO system due to the fact that the AO system does not respond instantaneously. It depends on the dynamic response of the controller and on the dynamic change in the aberrations of the eye [14]. In order to calculate the measurement and the bandwidth errors, it is necessary to first model the dynamic behavior of the adaptive optics system. The analysis presented here draws heavily from control theory, including the application of Laplace and z transforms. The reader unfamiliar with this material is referred to textbooks on control theory [15] and signal processing [16].

8.5.1 Modeling the Dynamic Behavior of the AO System

The dynamic behavior of an AO system can be modeled using the blocks displayed in Figure 8.2. [17]. First, the wavefront sensing camera stares at the residual wavefront for one sampling period. This is followed by a computational delay, τ_c, which corresponds to the lag between the moment the camera stops integrating and the time that the voltages are updated in the DM. This consists of the time taken to read the CCD, compute the centroids, multiply the centroids by the reconstruction matrix, and calculate the new voltages. The compensator calculates the voltages to be applied from the previous voltages and the reconstructed wavefront. Typically, the compensator consists of an integral controller of the form

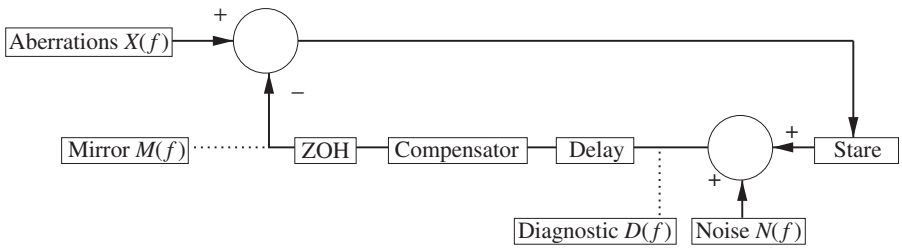

FIGURE 8.2 Schematic of the control loop.

$$y[\mathrm{n}] = y[\mathrm{n}-1] + Ku[\mathrm{n}] \tag{8.3}$$

where K is a variable loop gain, $y[\mathrm{n}]$ is the output from the compensator, and $u[\mathrm{n}]$ is the input to the compensator at time n. The transfer function of the integral compensator can be written as:

$$H_{\mathrm{COMP}}(z) = \frac{K}{1 - z^{-1}} \tag{8.4}$$

where z is the complex z-transform variable. Equation (8.4) can be rewritten in the Laplace domain by substituting $z = e^{sT}$. Finally, the mirror is held in position for one sampling period. This is called a zero-order hold because it is a zeroth-order (constant) approximation to the temporal evolution of the wavefront.

The transfer functions of the individual blocks are as follows:

1. Camera stare and the zero-order hold with sampling period $T = 1/f_s$, where f_s is the sampling frequency:

$$H_{\mathrm{STARE}}(s) = H_{\mathrm{ZOH}}(s) = \frac{1 - e^{-sT}}{sT} \tag{8.5}$$

2. Computational delay time τ_c:

$$H_{\mathrm{DELAY}}(s) = e^{-s\tau_c} \tag{8.6}$$

3. Integral compensator with gain K:

$$H_{\mathrm{COMP}}(s) = \frac{K}{1 - e^{-sT}} \tag{8.7}$$

In the above equations, $s = i2\pi f$ is the complex frequency variable, where f is the frequency and $i = \sqrt{-1}$. In what follows, all the blocks will be written with f as the argument, since f has a more intuitive meaning than s and is computed directly from the discrete Fourier transform (DFT) of the diagnostic data from the AO system. In order to calculate the wavefront errors, we must convert centroid measurements from diagnostics into wave aberrations. The residual mirror commands are the corrections to the current mirror position that would be applied if the loop gain were equal to unity. If the reconstruction matrix is **R** and the vector of centroid measurements is s, then the residual mirror commands, **v**, are given by $\mathbf{v} = \mathbf{Rs}$. Then, using the relationship between the mirror commands (actuator voltages) and the induced wavefront, we obtain a wave aberration at the position of each actuator. For continuous DMs, cross talk between the actuators can be well-modeled as a convolution

of the actuator voltages with the response of the neighboring actuators to the applied voltage [18].

The entire feedback arm of the loop, $H(f)$, can be written as the product of all the blocks:

$$H(f) = H_{\text{STARE}}(f) H_{\text{DELAY}}(f) H_{\text{COMP}}(f) H_{\text{ZOH}}(f) \tag{8.8}$$

There are two inputs into the control system: aberrations of the eye, $X(f)$, and the noise, $N(f)$, which is assumed to be white (same power at all temporal frequencies). Likewise, there are two outputs: the mirror position, $M(f)$, and the residual mirror commands obtained in the diagnostics, $D(f)$. The position of the diagnostics in the control loop is just after the addition of the noise, while the mirror position is just after the zero-order hold. For notational simplicity, we consider the noise to be input before, rather than after, the stare. This assumption has little impact on the transfer function of the control loop.

The transfer functions relating the outputs (the mirror position and centroid diagnostics) to the inputs (the aberrations of the eye and measurement noise) are

$$D(f) = \frac{1}{1 + H(f)} (X(f) + N(f)) \tag{8.9}$$

and

$$M(f) = \frac{H(f)}{1 + H(f)} (X(f) + N(f)) \tag{8.10}$$

Figure 8.3 plots the modulus squared of these transfer functions for a hypothetical adaptive optics system with the following parameters: $T = 0.05\,\text{s}$, $\tau_c = 0.05\,\text{s}$, and $K = 0.25$.

8.5.2 Computing Temporal Power Spectra from the Diagnostics

The time series of the residual wavefront at each actuator location is converted to a power spectrum using the DFT. In practice, the FFT is often used for speed of computation. The definition of the DFT used in this chapter is

$$D(p) = \frac{1}{\sqrt{\text{P}}} \sum_{\text{n}=1}^{\text{P}} d[\text{n}] \exp\left[\frac{-i2\pi(\text{p}-1)(\text{n}-1)}{N}\right] \tag{8.11}$$

where P is the number of diagnostic frames. This definition maintains power of the coefficients equal in either domain, that is,

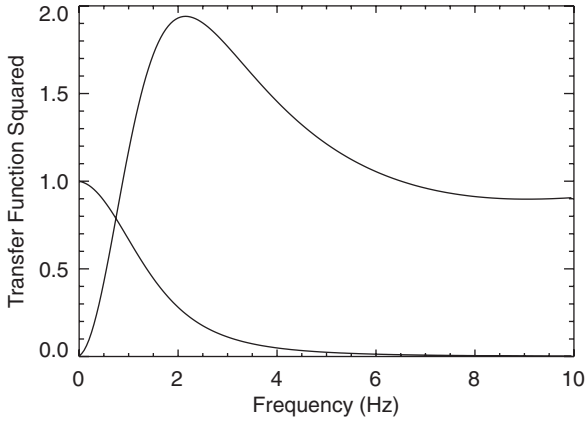

FIGURE 8.3 Plots of $|1/(1 + H(f))|^2$ (*top curve*) and $|H(f)/(1 + H(f))|^2$ (*bottom curve*).

$$\sum_{\mathrm{p}=1}^{\mathrm{P}} D(p)^2 = \sum_{\mathrm{n}=1}^{\mathrm{P}} d[\mathrm{n}]^2 \tag{8.12}$$

The power spectrum of the diagnostics is taken using the discrete Fourier transform:

$$|D(p)|^2 = |\mathrm{DFT}[d[\mathrm{n}]w[\mathrm{n}]]|^2 \tag{8.13}$$

where $w[\mathrm{n}]$ is a windowing function used to avoid spectral leakage due to the nonperiodicity of $d[\mathrm{n}]$, the residual wavefront as measured by the diagnostics. To convert to frequency space, we use the relationships

$$D(f) = D(f_s \mathrm{p}/\mathrm{P}) \tag{8.14}$$

and

$$D(-f) = D(f_s - f_s \mathrm{p}/\mathrm{P}) \tag{8.15}$$

Common windows include the Hanning, Hamming, and Blackman–Harris windows. There is a trade-off in eliminating the effect of spectral leakage at the expense of a reduction in spectral resolution inherent in each window. Care must be taken to scale $w[\mathrm{n}]$ to ensure that the average power in the window is unity:

$$\sum_{\mathrm{n}=1}^{\mathrm{P}} w[\mathrm{n}]^2 = \mathrm{P} \tag{8.16}$$

The power spectrum is then averaged over all the actuators and, if possible, over several sets of power spectra from the same eye. While the power spectrum is used to compute the error terms, the power spectral density (PSD) is often used for plotting purposes. The PSD is a continuous function with dimensions of wavefront squared per hertz and is obtained by dividing the power spectrum by P*T*. The PSD is usually displayed with the positive frequencies doubled and the negative frequencies discarded.

Another number of interest is the crossover frequency, which is defined to be the lowest frequency at which there is no correction. In Figure 8.3 this occurs at 1 Hz. In practice, it is usually determined by plotting the closed-loop power spectrum superimposed on the open-loop power spectrum and determining where these two curves first cross [19].

8.5.3 Measurement Noise Errors

The measurement noise squared error, σ^2_{NOISE}, is given by:

$$\sigma^2_{\text{NOISE}} = \sum \left| \frac{H(f)}{1+H(f)} \right|^2 |N(f)|^2 \tag{8.17}$$

where the summation is for all the discrete values of $f \in [-f_s/2, f_s/2)$.

The noise power spectrum may be computed from first principles using knowledge of the spot size, the light level, and the characteristics of the WS camera, such as the dark current and readout noise [20].

Alternatively, the noise can be calculated from the power spectrum. By inspection of Figure 8.3, it can be seen that the loop transfer function for the noise as seen by the diagnostics is close to unity at high frequencies. If the noise power is dominant over the aberration power at high temporal frequencies, the noise is given by the value of the power spectrum in the region close to half the sampling frequency. One can tell if this is the case by verifying that the power spectrum follows the $|H(f)/(1 + H(f))|^2$ curve at high frequencies. Since the noise is assumed to be white, this is an estimate of $N(f)$ at all frequencies.

Figure 8.4 plots the PSD of the residual aberrations using data from Keck Observatory's astronomical AO system. The PSD value of $|N(f)|^2$ may be read from the plot as the value of the PSD for $f = 200$ Hz, converted to a power spectrum value and inserted in Eq. (8.17) to calculate the measurement noise error. Inserting the value of the noise floor from the diagnostics into Eq. (8.17) gives

$$\sigma^2_{\text{NOISE}} = \sum \left| \frac{H(f)}{1+H(f)} \right|^2 |D(f_s/2)|^2 \tag{8.18}$$

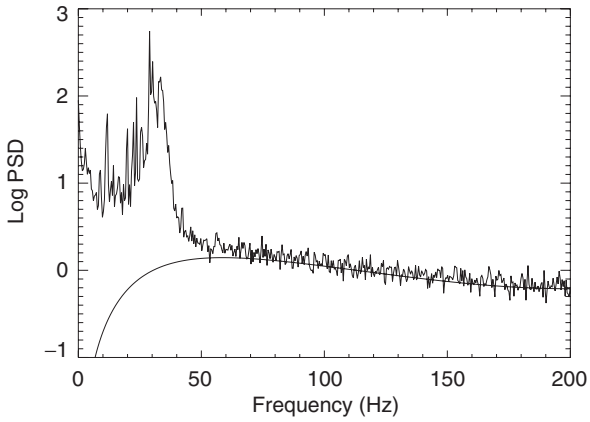

FIGURE 8.4 Power spectral density in nanometers squared per reciprocal hertz of the residual aberrations using the residual centroid measurements obtained at Keck Observatory. The theoretical noise curve is superimposed.

8.5.4 Bandwidth Error

The bandwidth squared error is given by:

$$\sigma_{\mathrm{BW}}^2 = \sum \left| X(f) - \frac{H(f)}{1+H(f)} X(f) \right|^2 = \sum \left| \frac{X(f)}{1+H(f)} \right|^2 \tag{8.19}$$

The diagnostics measure the bandwidth error with an added noise term due to the noise on the centroid measurement propagating through the control loop:

$$D(f) = \frac{X(f)+N(f)}{1+H(f)} \tag{8.20}$$

Combining Eqs. (8.19) and (8.20) gives the bandwidth squared error:

$$\sigma_{\mathrm{BW}}^2 = \sum \left(|D(f)|^2 - \left| \frac{1}{1+H(f)} \right|^2 |N(f)|^2 \right) \tag{8.21}$$

and it is evaluated by inserting the measured values of $|N(f)|^2$ and $|D(f)|^2$ into Eq. (8.21).

8.5.5 Discussion

The gain, K, and frame rate, f_s, should be chosen so as to minimize the sum of the bandwidth and measurement error terms, which depend on the temporal power spectrum of the eye aberrations and the brightness of the spots on the WS, respectively. The optimal trade-off can be achieved by calculating the two terms using residual centroids and a dynamic model of the system or simply by adjusting the parameters and evaluating the image quality. If the measurement error term dominates, then the frame rate or gain should be reduced. In addition, one would think about improving the centroiding algorithm. The accuracy of the slope estimate can be improved by implementing background subtraction (and reducing the background), flat-fielding, removing bad pixels, optimizing the area over which the centroid is calculated, and using maximum correlation instead of a centroid algorithm. On the other hand, if the bandwidth error dominates, then increasing the frame rate or the loop gain (up to a point) is beneficial. In addition, an improved controller design may reduce the bandwidth error [17, 21].

8.6 ADDITION OF WAVEFRONT ERROR TERMS

If all the error terms are statistically independent, then the total error is equal to the sum in quadrature of the individual error terms:

$$\sigma_{\text{TOTAL}} = \sqrt{\sigma^2_{\text{CALIB}} + \sigma^2_{\text{FITTING}} + \sigma^2_{\text{BW}} + \sigma^2_{\text{NOISE}}} \tag{8.22}$$

Using the Maréchal approximation,

$$S_{\text{TOTAL}} = S_{\text{CALIB}} S_{\text{FITTING}} S_{\text{BW}} S_{\text{NOISE}} \tag{8.23}$$

where, for instance, S_{NOISE} is the Strehl degradation due to the noise wavefront error variance, $e^{-\sigma^2_{\text{NOISE}}}$. The fact that the error terms are added in quadrature implies that the total error is dominated by the largest error terms and small terms have a negligible effect on the image quality. It is more important to accurately measure and, where possible, mitigate the large error terms rather than focusing on small sources of error.

Other aberrations that might have a significant bearing on the error budget are chromatic aberration if the wavefront sensing occurs at a different wavelength to the science imaging and anisoplanatism, which occurs when the light takes a different path to the science camera relative to the WS.

Acknowledgments This work was performed under the auspices of the U.S. Department of Energy by the University of California, Lawrence Livermore National Laboratory, under contract W-7405-Eng-48. The work has been supported by the National Science Foundation Science and Technology Center for Adaptive Optics, managed by the University of California at Santa Cruz

under cooperative agreement No. AST-9876783. Marcos van Dam received a CfAO minigrant to visit Don Miller's Lab at the Indiana University School of Optometry.

REFERENCES

1. Hardy JW. *Adaptive Optics for Astronomical Telescopes*. New York: Oxford University Press, 1998.
2. Roberts Jr L, Perrin MD, Marchis F, Sivaramakrishnan A, Makidon RB, Christou JC, Macintosh BA, Poyneer LA, van Dam MA, Troy M. Is That Really Your Strehl ratio. In: Bonaccini D, Ellerbroek BL, Ragazzoni R, eds. *Advancements in Adaptive Optics. Proc. SPIE*. 2004; 5490: 504–515.
3. Goodman J. *Introduction to Fourier Optics*. San Francisco: McGraw-Hill, 1968.
4. Gerchberg R, Saxton W. A Practical Algorithm for the Determination of Phase from Image and Diffraction Plane Picture. *Optik*. 1972; 35: 237–246.
5. Fienup JR. Phase Retrieval Algorithms: A Comparison. *Appl. Opt.* 1982; 21: 2758–2769.
6. Lane RG, Fright WR., Bates RHT. Direct Phase Retrieval. *IEEE Trans. Acoust., Speech, Signal Processing*. 1987; ASSP-35: 520–526.
7. Gonsalves RA. Phase Retrieval and Diversity in Adaptive Optics. *Opt. Eng.* 1982; 21: 829–832.
8. Paxman RG, Fienup JR. Optical Misalignment Sensing and Image Reconstruction Using Phase Diversity. *J. Opt. Soc. Am. A*. 1988; 5: 914–923.
9. Paxman RG, Schulz TJ, Fienup JR. Joint Estimation of Object and Aberrations by Using Phase Diversity. *J. Opt. Soc. Am. A*. 1992; 9: 1072–1085.
10. Loefdahl MG, Scharmer GB. Wavefront Sensing and Image Restoration from Focused and Defocused Solar Images. *Astron. Astrophys. Suppl. Ser.* 1994; 107: 243–264.
11. Rigaut FJ, Véran J-P, Lai O. Analytical Model for Shack-Hartmann-Based Adaptive Optics Systems. In: Bonaccini D, Tyson RK, eds. *Adaptive Optical System Technologies. Proc. SPIE*. 1998; 3353: 1038–1048.
12. Southwell WH. Wave-front Estimation from Wave-front Slope Measurements. *J. Opt. Soc. Am.* 1980; 70: 998–1006.
13. Tyler GA. Reconstruction and Assessment of the Least-Squares and Slope Discrepancy Components of the Phase. *J. Opt. Soc. Am. A*. 2000; 17: 1828–1839.
14. Hofer H, Artal P, Singer B, Aragón JL, Williams DR. Dynamics of the Eye's Wave Aberration. *J. Opt. Soc. Am*. 2001; 18: 497–506.
15. Franklin GF, Powell JD, Emami-Naeini A. *Feedback Control of Dynamic Systems*. Reading, MA: Addison-Wesley, 1998.
16. Oppenheim AV, Schafer RW. *Discrete-Time Signal Processing*. Upper Saddle River, NJ: Prentice Hall, 1999.
17. Madec P-Y. Control Techniques. In: Roddier F, ed. *Adaptive Optics in Astronomy*. Cambridge: Cambridge University Press, 1999, pp. 131–154.

18. Oppenheimer BR, Palmer D, Dekany RG, Sivaramakrishnan A, Ealey MA, Price TR. Investigating a Xinetics Inc. Deformable Mirror. In: Tyson RK, Fugate RQ, eds. *Adaptive Optics and Applications*, *Proc. SPIE*. 1997; 3126: 569–575.
19. Hofer H, Chen L, Yoon GY, Singer B, Yamauchi Y, Williams DR. Improvement in Retinal Image Quality with Dynamic Correction of the Eye's Aberration. *Opt. Express*. 2001; 8: 631–643.
20. van Dam MA, Le Mignant D, Macintosh BA. Performance of the Keck Observatory Adaptive-Optics System. *Appl. Opt.* 2004; 43: 5458–5467.
21. Dessenne C, Madec P-Y, Rousset G. Optimization of a Predictive Controller for Closed-Loop Adaptive Optics. *Appl. Opt*. 1998; 37: 4623–4633.